Role of local order in the small-scale plasticity of model amorphous materials

C. Fusco, T. Albaret, and A. Tanguy
Université de Lyon, F-69622 Lyon, France
and CNRS, UMR5586, Laboratoire de Physique de la Matiere Condensée et Nanostructures, Université Lyon 1, Domaine Scientifique de La Doua, F-69622 Villeurbanne Cedex, France
(Received 3 June 2010; revised manuscript received 14 October 2010; published 21 December 2010)

The mechanism of plastic flow in amorphous solids involves nucleation-controlled shear transformations, triggered under stress from fertile sites. However, the origin of these sites is still a matter of debate. In this paper, we show that the connection between local plastic activity and coordination defects in amorphous systems depends on the nature of the interatomic interactions. In particular, the directionality of the bonds, as quantified by the three-body term in Stillinger-Weber-like interactions, affects not only the role of local defects, but also the size of the plastic rearrangements, and the global stress-strain behavior. We study the effect of structure changes due to different quenching rates as well. We conclude the paper by a comparison between amorphous plasticity and the Peierls-Nabarro theory of plasticity in crystals.

DOI: 10.1103/PhysRevE.82.066116 PACS number(s): 62.20.F−, 61.43.−j, 81.05.Kf

I. INTRODUCTION

The microscopic origin of the plastic deformation in amorphous solids is not so well understood as plasticity in crystals. In crystals, the plastic deformation is supported by linear defects, the dislocations, whose interactions and nucleation processes are now well known [1]. Moreover, the regularity of the lattice in crystals allows to perform exact calculations, as for the Peierls-Nabarro Theory of yield stress [2,3] where the width of the dislocation and the directionality of the bonds is shown to play a crucial role in the quantitative value of the critical stress for dislocation motion. In the case of amorphous solids, the nature of defects is currently identified as local shear [4], shear transformation [5], or shear transformation zone [6], with a spatial organization triggered under an external stress, which is still a matter of active debate [6–14]. The nucleation of these active sites, as well as their interaction during plastic deformation is not well understood: is it possible to identify a local structural criterion for plasticity [12–17], or are the plastic rearrangements mainly triggered by long range interactions [8,12]? What are the mechanisms responsible for the propagation of the plastic rearrangements? Do they propagate through elastic cascades [11,12], statistical interactions [6,7], collective instability [4], or history-dependent structural changes in the material [10,18]? Moreover, the stress-strain behavior is sometimes characterized by strain softening and inhomogeneous plastic flow. However, the microscopic origin of the strain softening in disordered solids is not yet understood [13,15,19–23].

In this paper, we study the elastoplastic response of a model glass in the athermal limit, with the help of quasistatic classical simulations. The model glass is inspired by classical descriptions of amorphous silicon (A-Si). It is described through empirical interactions with two and three-body interactions [24], and is submitted to an external shear. Tuning the three-body contribution in the interatomic interactions allows us to study the systematic effect of local order and directionality of the bonds on the mechanical response of the system. Different quenching rates have also been compared for the preparation of the initial configurations, in order to enhance the effect of the initial structure on the mechanical response. The paper is organized as follows: in the first part we describe the numerical details, in the second part we compare the global stress-strain behavior of our different samples, we then propose a method to analyze quantitatively the local plastic rearrangements in the system. In the last part, we insist on the different roles played by local coordination defects and on their restricted connection with local plastic rearrangements. Finally, we conclude by providing a qualitative comparison with the Peierls-Nabarro theory of plastic yield in crystals.

II. PREPARATION OF THE AMORPHOUS SILICON MODEL AND COMPUTATIONAL DETAILS

We consider a model amorphous silicon (A-Si) consisting of 32 768 atoms contained in a cubic box with lengths $L_x = L_y = L_z$ of approximately 87 Å. In order to generate the amorphous structure we use a procedure similar to that outlined in Refs. [26,27]. An initial Si crystalline configuration is heated up to the liquid state and equilibrated at 3500 K; afterward, we perform a quench with quenching rates between 10^{11} and 10^{14} K/s. When a temperature of about 10 K is reached, the quenching procedure is stopped and a potential energy minimization with respect to the atomic positions is performed. The minimization is done using the Polak-Ribiere version of the conjugate gradient algorithm, using the backtracking method described in Nocedal and Wright's numerical optimization [29]. The minimization is stopped when all the force components are below 10^{-3} eV/Å. In the heating, quenching, and minimization procedures the Si atoms interact via the Tersoff potential [25]. In this way we obtain the initial configurations that we use in the study of the mechanical response of A-Si.

In order to analyze the effect of the local order on the plastic response we have considered the mechanical behavior of A-Si where the Si-Si interaction is described by the Stillinger-Weber (SW) potential [24], where we have tuned the prefactor of the three-body term λ. We have studied the mechanical response of the system for values of λ ranging

 ©2010 The American Physical Society

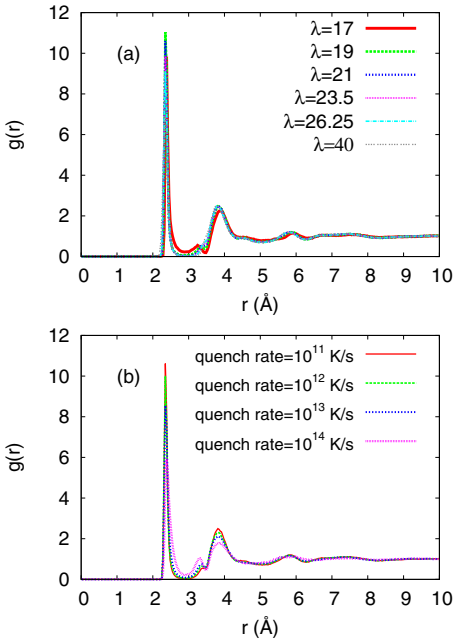

FIG. 1. (Color online) Radial distribution for different values of λ and quenching rate 10^{11} K/s (a), and for different quenching rates and λ=21 (usual SW potential) (b).

from 17 to 40 (for the usual SW potential λ=21). In this way we can tune the bond directionality, favoring local order, in our system. In order to obtain initial 0 K configurations of A-Si for different values of λ we have annealed the initial Tersoff configuration, generated with the procedure described above, using a Berendsen thermostat [30] at 100 K for 10 ps for all the considered values of λ and SW potential. Then the thermostat has been switched off and the system has been minimized with the same procedure used for the Tersoff potential. Extra 0 K configurations of A-Si have also been obtained by applying a Berendsen barostat while annealing the initial Tersoff configurations at 100 K and during the subsequent minimization procedure up to 0 K. The Berendsen barostat ensures that an optimal volume of the box is found, which gives a very low residual pressure. Other initial A-Si configurations have been generated by applying the same procedure, but annealing at 120 K instead of 100 K. The radial distribution functions corresponding to the initial configurations with different λ and quenching rates are shown in Fig. 1. As it can be seen in Fig. 1(a) almost all the curves show a higher peak at $r=2.34$ Å, corresponding to the first-neighbors distance. Smaller peaks appear at $r=3.8$ Å and $r=5.8$ Å. A smaller shoulder at $r=3.35$ Å is also observed, which corresponds to the tendency of the SW potential to form fivefold coordinated defects. Regarding the effect of the quenching rate on the structure of the initial configurations, we see that the height of the first peak, located at $r=2.34$ Å, tends to increase and that of the first minimum, located at $r\simeq 2.88$ Å, tends to decrease by decreasing the quenching rate. This is a signature of a more solidlike structure for low enough quenching rates; on the other hand, if the starting liquid configuration is quenched very fast (e.g., quenching rate 10^{14} K/s) the first minimum is sensibly larger than zero and the shoulder is much more pronounced, resembling a more liquidlike structure. These preliminary considerations are quite important for the understanding of the role played by the structure in the plastic response of the system. The main structural properties of the amorphous configurations we have obtained are reported in Table I (for several values of λ and quenching rate 10^{11} K/s) and in Table II (for different quenching rates and λ=21). After having presented the method we used to generate the initial configurations, we briefly comment on the choice of the Tersoff potential for the initial quenching procedure. This was motivated from a previous work from Ref. [27] in which this potential is employed with success to obtain A-Si structures in reasonable agreement with experimental structure factors. Moreover, even at quenching rate of 10^{11} K/s the Stillinger-Weber potential is known to lead to configurations too close to the liquid state showing a large angle deviation as well as an excess of fivefold coordinated defects which lead to an extra peak in the radial distribution

TABLE I. Comparison of structural properties for A-Si for different values of the prefactor λ of the three-body term of the SW potential. The configurations are obtained with a quenching rate of 10^{11} K/s.

Property	λ=17	λ=19	λ=21	λ=23.5	λ=26.25	λ=40
Average coord.	4.35	4.11	4.08	4.06	4.05	4.00
Average angle	107.06	108.53	108.81	108.93	109.02	109.21
Angle Dev.	17.54	12.92	11.92	11.43	11.03	9.72
C44 (GPa)	25.63	29.38	34.24	39.38	44.35	64.88
B0 (GPa)	107.28	99.3	100.59	103.48	106.81	121.12
ν	0.389	0.365	0.347	0.331	0.318	0.273
Density (g/cm^3)						
Without barostat	2.30277	2.30277	2.30277	2.30277	2.30277	2.30277
With barostat	2.33915		2.2953			2.248433
Pressure (GPa)						
Without barostat	−1.82	−0.096	0.638	1.38	2.1	5.07
With barostat	−0.011168		0.01331			−0.1142

TABLE II. Comparison of structural properties for A-Si for different quenching rates with $\lambda=21$.

Property	10^{11} K/s	10^{12} K/s	10^{13} K/s	10^{14} K/s
Average coord.	4.08	4.12	4.19	4.39
Average angle	108.81	108.50	108.1	106.96
Angle Dev.	11.92	13.69	15.52	19.46
C44 (GPa)	34.24	32.04	29.98	27.66
B0 (GPa)	100.59	105.19	108.71	118.57
ν	0.347	0.362	0.374	0.392
Density (g/cm^3)	2.30277	2.32238	2.32238	2.32238
Pressure (GPa)	0.638	1.34	1.019	−0.8787

function [31] which is not observed in the experiments [32].

We have studied the plastic response of A-Si for the different initial configurations by applying a shear strain in the x direction in the quasistatic limit. To reach this limit, we apply successive stepwise incremental homogeneous elementary shear strains of step size $\delta\epsilon=10^{-3}$ (corresponding to an elementary displacement of $\delta x=2\delta\epsilon L_y=0.1745$ Å). After each strain step, the sample is then relaxed by using the same minimization procedure as described above. This procedure assumes that the system has enough time to relax between two consecutive shear steps, that is the case in a quasistatic loading at very low temperature. It has been proven recently that this procedure is the exact quasistatic limit of a finite shear rate deformation at very low temperature [33]. For each configuration, we have considered a series of 250 elementary strain displacements, corresponding to a total displacement of 50% of the length of the system. In the following, we will refer to shear strain as the ratio $\delta x/L_y$, so that the maximum strain applied is 50%. The preparation of the initial configurations and the quasistatic shear dynamics has been done using the open source LAMMPS molecular dynamics simulation package [34], enabling us to perform parallel calculations on the different configurations.

III. STRESS-STRAIN RELATIONSHIP

In order to probe the elastic and plastic response of the system for different values of the prefactor λ of the three-body term of the SW potential we have computed the shear stress as a function of the applied strain for all the values λ considered. The stress tensor $\sigma_{\alpha\beta}$ was computed in the relaxed minimized configuration from the derivative of the total energy E,

$$\sigma_{\alpha\beta}=-\frac{1}{V}\sum_i\sum_{j>i}\frac{\partial E}{\partial r_{ij}^{\alpha}}r_{ij}^{\beta}, \tag{1}$$

where $V=L_xL_yL_z$ is the total volume of the box and r_{ij}^{α} is the component along the α direction of the position vector between atoms i and j. Since we apply the strain along the x direction we are interested in the shear stress in the xy plane, i.e., σ_{xy}. Figures 2(a) and 2(b) show the evolution of the shear stress as a function of the applied strain for several values of λ and for different quenching rates, respectively.

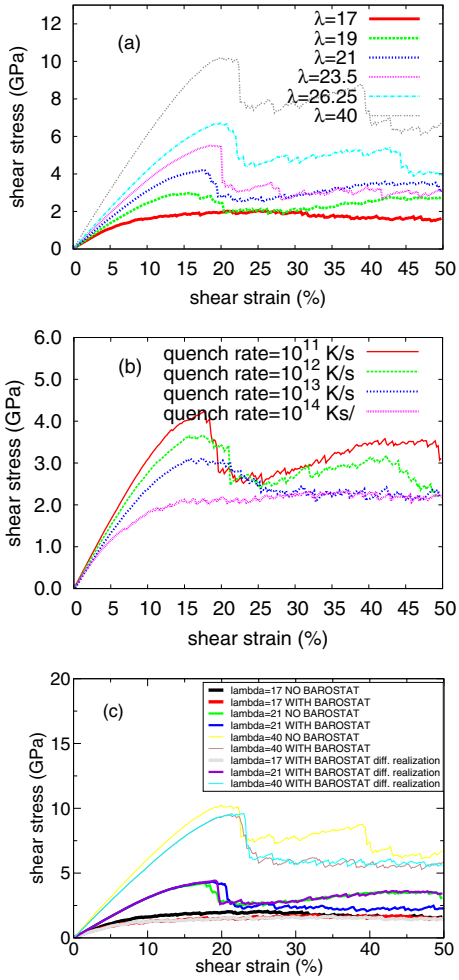

FIG. 2. (Color online) Shear stress vs shear strain for different values of λ and quenching rate 10^{11} K/s (a), for different quenching rates and $\lambda=21$ (usual SW potential) (b), and for different initial pressures—see Table I (c).

The general trend seen in Fig. 2(a) is that the shear stress increases as a function of λ. In the low strain regime all the curves display a linear behavior, whose slopes correspond to the values of the elastic constants C44 found for the different values of λ (see Table I): the higher the value of the three-body contribution the higher the slope is, thus the more rigid is the system. This is simply due to the fact that a higher prefactor in the three-body term produces higher energies associated to the angle distortions. The initial linear regime in the stress-strain relationship does not necessarily correspond to an elastic behavior because when the shear is applied some local irreversible rearrangements can take place in the system [4,26]. These rearrangements correspond to plastic events. They have been identified by applying a reverse strain step on the system and measuring the corresponding energy dissipation, as detailed in Sec. IV. In order to more clearly relate the stress-strain behavior to the microscopic dynamics of the system we have shown in Fig. 3 (left) the displacement field in a narrow z region of the system during an elementary strain step and for $\lambda=40$. At low strains [Fig. 3(a)] the displacements are heterogeneous although mainly reversible and linear with the applied strain. When

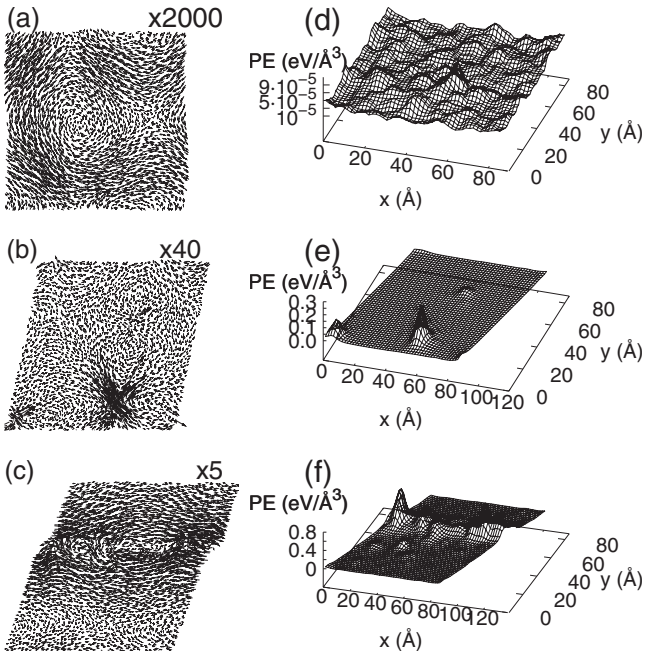

FIG. 3. Displacement field during an elementary strain step $\delta\epsilon = 10^{-3}$ in a narrow z region (40 Å $< z <$ 50 Å) for $\lambda = 40$ and shear strain = 1.6% (a), shear strain = 22% (b), shear strain = 40% (c). The displacements are magnified by a factor of 2000 (a), 40 (b), and 5 (c). (d) (e) and (f) are the corresponding values of PE(x,y) summed for different values of z (40 Å $< z <$ 50 Å).

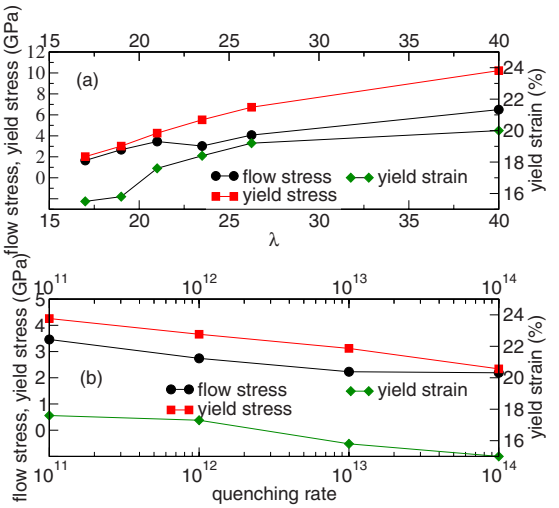

FIG. 4. (Color online) Dependence of the yield strain, of the flow stress and of the yield stress on the parameter λ for fixed quenching rate 10^{11} K/s (a), and on the quenching rate for λ = 21 (usual SW potential) (b).

the shear strain is increased some local irreversible rearrangements can be identified. Figure 3(b) shows a typical quadrupolar irreversible (plastic) event in the bottom part of the system. During the deformation, the plastic events tend to increase in number and after the breakdown point (or yield point), i.e., the location where the stress is maximum, they eventually give rise to elementary shear bands, spanning the whole system size. Note that several shear bands can appear during the plastic deformation, for example around 22% just after the previously described quadrupolar event, or as displayed in Fig. 3(c) at strain 40% when another large stress drop is observed. As it can be seen, the shear band is due to an alignment of vortices along the shear direction, as usual in disordered systems [4,28].

The three prototypical displacement configurations shown in Fig. 3 for λ = 40 are quite generic, and the same kind of patterns has been seen for the other values of λ that we have studied. The dependence of the yield strain (strain at which the stress is maximum) and of the flow stress (average value of the shear stress in the last 10% of the shear-stress curves, in the plastic plateau) on λ and on the quenching rate are shown in Fig. 4. As it can be seen from Fig. 2, it is difficult to extract a univocal value of the flow stress because for such a small system size [4] the plateau of the stress-strain curves exhibits large fluctuations and steps, which are a signature of a high plastic activity and of the occurrence of shear bands. In particular the stress tends to increase in some cases for high strains (for example the flow stress for λ = 21 is larger than that for λ = 23.5) giving rise to the dip in the flow stress vs λ curve as seen in Fig. 4(a). There is however a clear tendency for both the yield strain and the flow stress to increase with λ, and the value of λ = 21 appears as an inflexion point for the yield and for the flow stresses, suggesting two different kinds of mechanical behaviors for small (λ < 21) or large (λ > 21) values. Noticeably, at the yield point the stress has an abrupt drop for high values of λ, while by decreasing λ this drop becomes less sharp and for low λ no drop at all is observed; in the latter case the stress increases smoothly with the strain as it has been already observed in the case of a purely two-body interaction [4]. The same qualitative behavior is observed by varying the quenching rate. If the system is cooled down slowly from the liquid an amorphous solid is formed and a drop in the stress is found at the yield point, which becomes smoother for higher cooling rates. At the highest cooling rate we have used (10^{14} K/s), the stress-strain curve becomes very smooth, suggesting the importance of the detailed structure in the mechanical response of the system. Finally, the study of the initial pressure dependence shows a tendency for the flow to be stabilized when the initial pressure is smaller, especially for higher values of λ-see Fig. 2(c).

IV. DETERMINATION OF PLASTIC REARRANGEMENTS

In order to identify the plastic events in our system we have developed a method that allows us to determine which are the plastically active regions in the sample on the basis of the comparison between initial and reverse configurations at each strain step. The reverse configuration at strain step ϵ_i is obtained by starting from the minimized configuration at strain ϵ_{i+1} and by performing a backward minimization at strain ϵ_i. The backward minimization corresponds to an elastic relaxation and the comparison between the initial and reverse configuration defines the plastic energy,

$$E_i^{plastic} = E_i^{ini} - E_i^{rev}, \tag{2}$$

where E_i^{ini} is the energy of the initial configuration at ϵ_i, and E_i^{rev} is the energy of the reverse configuration at the same

strain ϵ_i. In order to spatially identify a plastic event, and discuss the localization and the spatial organization of plastic events into shear bands, we introduce a quantity that we call the "atomic plastic energy." This local quantity is computed on each atom during a forward and backward deformation as an irreversible sum over the pair and three-body contributions. It is defined as

$$PE_{at}(i_a) = \left[\sum_{j_a} |V^{2b}_{i_a,j_a}(\epsilon_i^{ini}) - V^{2b}_{i_a,j_a}(\epsilon_i^{rev})|^2 + \sum_{j_a} \sum_{k_a} |V^{3b}_{j_a,i_a,k_a}(\epsilon_i^{ini}) - V^{3b}_{j_a,i_a,k_a}(\epsilon_i^{rev})|^2 \right]^{1/2}, \quad (3)$$

where $V^{2b}_{i_a,j_a}$ is the two-body energy due to the interaction between atoms i_a and j_a, and $V^{3b}_{j_a,i_a,k_a}$ is the three-body contribution from the triplet j_a,i_a,k_a in which i_a is the central atom. The local quantity $\mathrm{PE}_{at}(i_a)$ is not affected by block motions (translations or rotations), but it reflects irreversible changes in the bond length and/or angle. In order to obtain a continuous field from the atomic plastic energy we used a coarse-graining procedure similar to Ref. [35]. We thus define a density of plastic energy $\mathrm{PE}(r)$ by

$$\mathrm{PE}(r) = \sum_{i_a} \mathrm{PE}_{at}(i_a) \left(\frac{1}{(\pi\omega^2)^{3/2}} \exp - \frac{|r - r_{i_a}|^2}{\omega^2} \right) \quad (4)$$

where ω is the characteristic Gaussian width ($\approx$2.6 Å) which corresponds approximately to the first neighbor distance. Typical examples of $\mathrm{PE}(r)$ on a plane are shown in Figs. 3(d)–3(f) for shear strains of 1.6%, 22%, and 40%, respectively, in the case $\lambda=40$. Elementary plastic events are identified from the local maxima of the density $\mathrm{PE}(r)$, and we define their intensities by summing of the density of plastic energy [Eq. (4)] over their basin. A basin [36] is formed by the region of space traversed by all the paths along the gradient direction $\vec{\nabla}\mathrm{PE}(r)$ that terminate at the same local maximum of $\mathrm{PE}(r)$. Therefore the basins associated to different local maxima [the attractors of $\mathrm{PE}(r)$] form disjoint regions of space over which $\mathrm{PE}(r)$ can be summed.

In order to practically determine the attractors of $\mathrm{PE}(r)$ as well as their basins and the corresponding intensity, we used a simple methodology already described in Ref. [37] in which we write the density of plastic energy on a $(100 \times 100 \times 100)$ 3D grid before performing a finite difference analysis. First the attractors are determined as the local maxima on the grid. The corresponding basin is then obtained by finding the grid points belonging to all the possible paths that start from an attractor grid point and along which the density $\mathrm{PE}(r)$ decreases. Because we use a finite grid, a single grid point close to the basin's surfaces can be shared by several basins. In this case the density on the grid point is equally divided between the basins it belongs to.

Following this procedure a set of elementary events is found for each configuration. Figure 5(a) gives an example of the spatial repartition of the density region for the basin of highest intensity for $\lambda=40$ at shear strain 40%. In Fig. 5(b) a similar plot for both the two basins of highest intensity is shown. As it is suggested by the large number of maxima with very low plastic energy densities seen in Fig. 3(d), our scheme may lead to a large number of elementary events (typically several hundreds) per configuration which may not all be significant to address the overall plastic properties of the amorphous material. To avoid the analysis of a large number of elementary events at each configuration we applied two additional criteria from which we selected only the most significant elementary events to which we will refer in the following as "plastic events." Our first criterion reflects the fact that at low shear strain, the reversible nonaffine field is associated to a large ensemble of attractors and basins of low intensity which lead to insignificant value of the plastic energy, due to numerical accuracy even after the reverse deformation ($E_i^{plastic} \lesssim 1$ meV). To get rid of these low intensity attractors which are typically represented by the two-dimensional projection in Fig. 3(d), we first ordered all the elementary events as a function of their intensity (i.e., the density summed over their basin). Then, we systematically discarded the low intensity elementary events starting from the lowest intensity event until we found an intensity difference from one event to the next one of at least +0.03 eV. This energy step in the intensity distribution of the elementary events indeed indicates the occurrence of a higher plastic activity with respect to the "sea" of events associated to the numerical accuracy accompanying the reversible nonaffine displacement field. Its value corresponds roughly to the contribution to the variation of energy due to forces within the numerical accuracy (10^{-3} eV/Å) during a cooperative displacement of a few tens of Å [39]. In our data, this value clearly separates large scale events to a sea of minor events, in the beginning of the deformation. Using this criterion the elementary events shown in a 2D projection in Fig. 3(d) are discarded while the most relevant ones as for example the main event shown in Fig. 3(e) are considered for further analysis. However, at large strains, all the elementary events can bear rather large intensities without large intensity difference between events. These tiny differences are not necessarily associated to small reversible displacements and numerical accuracy. In this case, the application of our first criterion may wrongly discard significant plastic events. To ensure that all significant events are always present in our analysis, we applied a second criterion which includes in the list of plastic events all the elementary events whose attractors are located at less than 3.4 Å (slightly larger than the

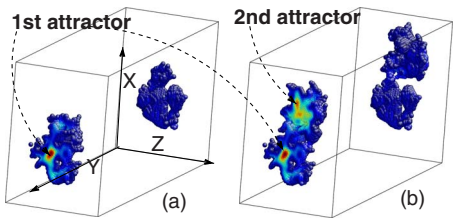

FIG. 5. (Color online) (a) Region of high plastic energy density for the most intense plastic event found at $\lambda=40$ and shear strain 40%; the color code ranges from blue to dark red (black to gray in the black and white version) which corresponds to a variation ranging from 20% of the maximum density, to the maximum density. The shear band here spans the plane (X,Z) (b) Region of high plastic energy density for the two most intense plastic events for the same configuration as in (a) with the same color code.

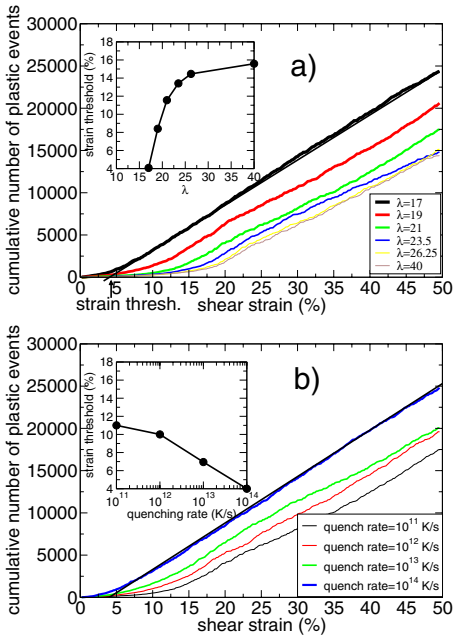

FIG. 6. (Color online) Cumulative number of plastic events as a function of the applied shear strain for different values of λ for a A-Si system prepared with a quenching rate of 10^{11} K/s (a) and for different quenching rates with λ=21 (b). The black lines are linear fits to the curves at large strains. In the insets, the strain threshold, defined from the linear fits of the curves at large strain.

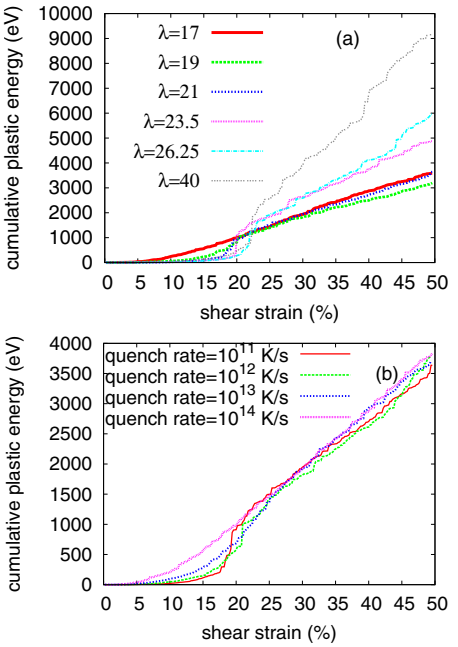

FIG. 7. (Color online) Cumulative plastic energy as a function of the applied shear strain for different values of λ for a A-Si system prepared with a quenching rate of 10^{11} K/s (a) and for different quenching rates with λ=21 (b).

size of the first neighbors shell) from an atom that displays a nonaffine displacement larger than 0.05 Å. This arbitrary value for the nonaffine displacement has been chosen by comparing the total PE(r) energy integrated over all the basins with the total dissipated energy $E_i^{plastic}$. It allows to consider all events contributing significantly to the dissipated energy, especially for high stresses, in the second part of the deformation process [39].

V. ANALYSIS OF THE PLASTIC REARRANGEMENTS

The evolution of the total number of plastic events with the applied strain is shown in Fig. 6. From this figure, it is clear that the total number of plastic events decreases by increasing λ and/or by decreasing the quenching rate. Furthermore we can identify a region at low strains where the number of plastic events does not increase significantly by increasing the applied strain. This allows to define a *strain threshold* (see inset) beyond which the increase of the number of plastic events is approximately linear with the applied shear strain. Interestingly this strain threshold increases with λ in accordance with the increase of the yield stress with λ shown in Fig. 4(a), and decreases with the quenching rate in accordance with the decrease of the yield stress with the quenching rate shown in Fig. 4(b). This indicates that the triggering of plastic rearrangements requires to overcome some energetic barriers which are possibly reduced by the application of the shear strain, but always increase with λ, or with a lower quenching rate. The sole number of plastic events, however, does not provide enough information on the mechanisms ruling the plastic response of A-Si. The plastic energy defined in Eq. (2) gives a measure of the energy dissipated in plastic rearrangements. If at a certain applied strain there are events contributing to a large increase in the plastic energy, we expect to find a corresponding large variation in the shear stress at that particular strain value. This is confirmed by looking at the behavior of the cumulative plastic energy as a function of the shear strain, displayed in Fig. 7 that can be compared to stress drops displayed in Fig. 2.

For low values of λ the plastic energy is very low at small shear strains and then it increases smoothly and linearly for larger applied strains. For larger λ we notice a dramatic increase of the plastic energy at the yield strain. The magnitude of this increase is larger for larger λ and reflects the strain softening observed in Fig. 2. We can also see that the fluctuations of the plastic energy in the high strain regime become more pronounced by increasing λ; such a behavior can be ascribed to the occurrence of localized plastic events and shear bands carrying a larger amount of plastic energy. A similar trend is found by decreasing the quenching rate. This kind of information cannot be deduced by simply looking at the evolution of the number of plastic events of Fig. 6, which shows only a smooth linear increase even for large values of λ or for small quenching rates, but must be related to the change in the nature of the plastic events with the applied strain.

We analyze now in detail the size and the spatial distribution of plastic events. We can estimate the size of a plastic event by using the method used to identify a plastic event, and looking at the decay of the intensity of an attractor as a function of the distance after angular average. We fit it with an exponential function whose exponential decay factor gives a measure of the size of the basin of the attractor, that

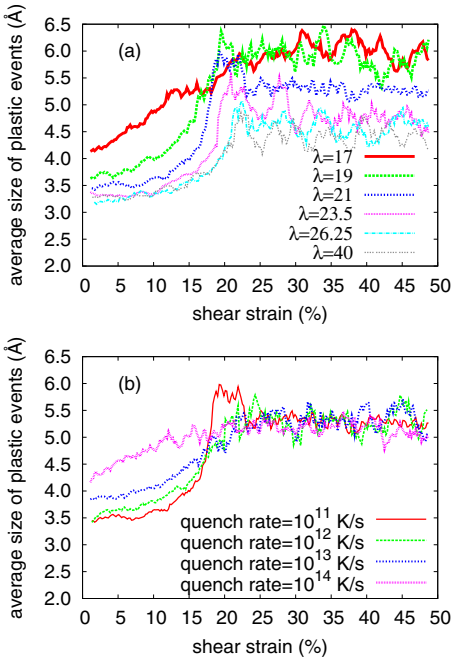

FIG. 8. (Color online) Average size of plastic events as a function of the applied shear strain for different values of λ for a A-Si system prepared with a quenching rate of 10^{11} K/s (a) and for different quenching rates with λ=21 (b). In order to reduce the statistical noise each data point has been averaged over ten shear steps.

we assume to be approximately the typical size of the corresponding plastic event. Repeating this procedure for all the attractors and averaging over all of them at each strain, we obtain the evolution of the average size of the plastic events with the applied shear strain, which is shown in Fig. 8. It can be seen that the average size tends to saturate at large strains, although large fluctuations are still visible. Moreover, the size of the plastic events generally decreases by increasing λ. Apart from λ=17 [Fig. 8(a)] and for quenching rate 10^{14} K/s [Fig. 8(b)], we observe a maximum in the size that is approximately located at the yield point. This indicates that at that point large plastic events occurs in the system, most probably arranged in a shear band, which is consistent with the microscopic dynamics as shown in the displacements in Fig. 3. For λ=17 the behavior is quite different, with few peaks located at different values of strain; in fact, in this case, many shear bands and large localized events occur at different places in the system and for relatively small applied strain, allowing to a progressive but almost homogeneous global deformation. This is very different for large λ. Combining the information from Fig. 6–8 we can argue that for low values of λ and/or for high quenching rates the plastic response is dominated by many large plastic events for which the rate of plastic energy is roughly constant (approximately linear increase of plastic energy with shear strain), while for larger values of λ and/or smaller quenching rates the plastic events become rarer and smaller in size, but they carry a large amount of plastic energy once the yield point has been reached. In other words, the elastic energy is accumulated and released abruptly at the yield strain for large λ and or small quenching rates; on the other hand, for small λ and/or large quenching rates the plastic energy is widespread through many more plastic rearrangements.

TABLE III. Yield stresses σ_Y, width of the plastic event at the yield point W and corresponding values of b obtained by using Eq. (5) for different values of λ for a A-Si system prepared with a quenching rate of 10^{11} K/s, and for different values of the quenching rate at λ=21.

λ	W (Å)	σ_Y (GPa)	b (Å)
17	6.11	2.01	1.64
19	6.11	2.80	1.75
21	5.63	4.23	1.75
23.5	5.13	5.47	1.67
26.25	4.73	6.64	1.59
40	4.57	10.13	1.59
Quench rate	**W (Å)**	**σ_Y (GPa)**	**b (Å)**
10^{11} K/s	5.63	4.23	1.75
10^{12} K/s	5.39	3.53	1.61
10^{13} K/s	5.39	3.0	1.56
10^{14} K/s	5.30	2.32	1.45

It is interesting at this point to compare the quantitative values obtained here in the case of amorphous solids with the estimation of the yield stress given by Peierls and Nabarro [2,3] in case of a single dislocation moving in a crystal. The Peierls stress σ^*_{xy} is given by

$$\sigma^*_{xy} = Ae^{-2\pi W/b}, \tag{5}$$

where $A=2C_{44}/(1-\nu)$ (ν is the Poisson ratio), W is the dislocation width and b is the Burgers vector, given by the interatomic spacing. We will consider in our case that W is given by the average size of the plastic events in the plastic flow part of the stress-strain curve. The Peierls stress is the force per unit surface needed to move a dislocation within a plane of atoms. It corresponds to the barrier needed to spread the plastic deformation along the solid. It can therefore be associated to the yield stress in our analysis. Although Eq. (5) was introduced in the context of dislocation theory in crystals we can try to apply it to our case for the motion of shear bands in amorphous solids in order to establish a relationship between the yield stress and the width of a shear band and to characterize the effect of the local order (through the parameter λ) on this relation. Therefore our assumption is that the isolated shear band behaves in a dislocationlike fashion. From the data of Tables I and II combined with the measurements of the yield stress σ_Y and of the width W, we get an estimation of $b(\lambda)$ given by Eq. (5). The results are reported in Table III for different values of λ and of the quenching rate.

Surprisingly enough, we see from Table III that the computed values of b are all in the same range b

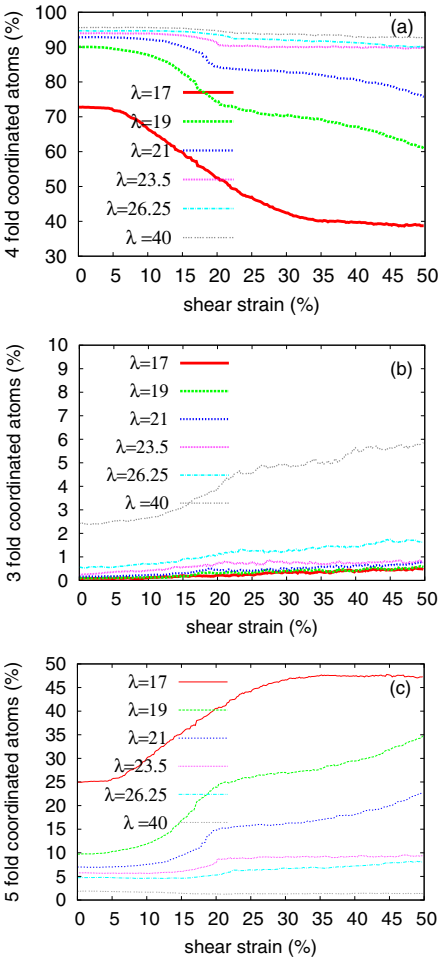

FIG. 9. (Color online) Percentage of fourfold (a), threefold (b), and fivefold (c) coordinated atoms as a function of the shear strain for several values of λ for a A-Si system prepared with a quenching rate of 10^{11} K/s. These coordination numbers were calculated by fixing a cutoff of 2.9 Å.

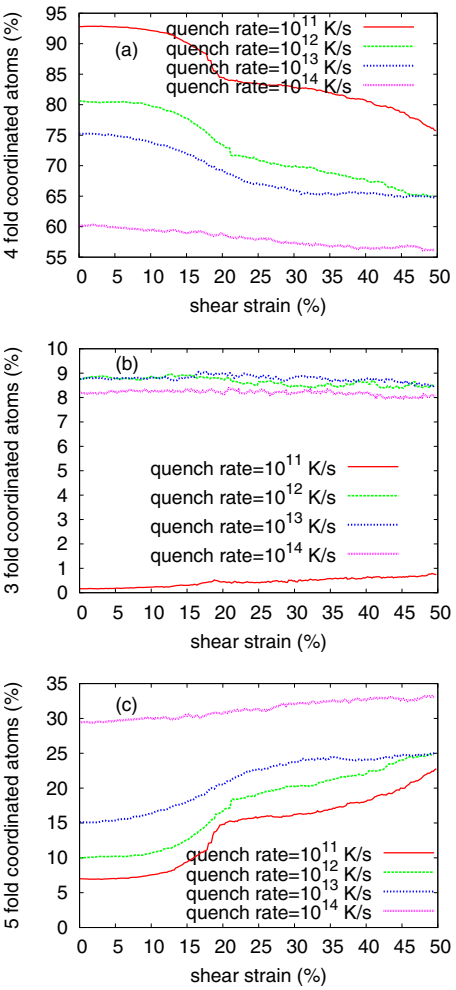

FIG. 10. (Color online) Same as Fig. 9 for different quenching rates with λ=21.

=1.6 Å ± 10%, independently of the value of λ and of the quenching rate. Moreover, *b* is comparable (while always smaller) to the interatomic distance. This result supports thus the description of plasticity in amorphous solids as a dislocationlike mechanism, where the elementary processes are strongly dependent on the local order, especially through their effective width *W*. In the following section we will study the connection between the location of elementary plastic events and structural defects in our samples.

VI. CORRELATION BETWEEN COORDINATION DEFECTS AND PLASTIC EVENTS

The coordination number of each atom is calculated by counting the number of neighbors within a cutoff radius of 2.9 Å, which is consistent with the tail of the first neighbor shell as seen in the radial distribution functions. The percentage of fourfold, threefold and fivefold coordinated atoms is plotted in Figs. 9 and 10 as a function of the applied shear strain for different values of λ and for different quenching rates, respectively. The coordination number that is the most representative of the system allows to define, by opposition, the structural *defects*. For the system at rest and λ ≥ 17, the majority of atoms is fourfold coordinated. We will thus consider in the following threefold and fivefold coordinated atoms as sites of structural *defects*. However, these percentages evolve with the applied strain. Generally the number of defects increases with the shear strain. It is not the case for pure two-body interactions, as in Lennard-Jones glasses. This increase is rather sharp at the yield strain when the system experiences more irreversible rearrangements. The percentage of defects created and the most dominant defects vary strongly with λ. For lower values of λ we observe a predominance of fivefold coordinated atoms, while for higher values of λ, threefold coordinated atoms dominate, since a stronger three-body term favors the atoms being far apart, in qualitative agreement with the findings of Ref. [26]. The environment of atoms is thus strongly λ dependent, and the defects created are not always "liquidlike" in contradiction to the schematic description in Ref. [15]. Interestingly, for λ =17 the number of defects overcomes the number of fourfold coordinated atoms already at a shear strain of 20% (in this case the percentage of defects reaches 60% after a deformation of 50%), while for the larger values of λ studied the fourfold coordinated atoms are always larger in number. If

we increase the quenching rate we also see from Fig. 10 that the number of defects increases. This is in agreement with the more disordered structure obtained by preparing the system with a faster quenching. In particular, fivefold defects become dominant for large quenching rates. The occurrence of plastic events might thus be related to the increase of the number of defects in the structure, for all the values of λ studied here [38].

We want now to quantify the propensity for a plastic event to localize near a structural defect, as a function of λ and of the quenching rate. For this purpose it is not sufficient to simply count the number of plastic events localizing on defect sites, since different structures may have different densities of defects. Therefore we must consider the ratio between the percentage of plastic events located on defect sites and the percentage of the corresponding defects. More precisely we introduce, at each applied strain ϵ_i, the following "correlation function" $C(\epsilon_i)$:

$$C(\epsilon_i) = \frac{p_{pe}^{defn}}{p^{defn}}, \tag{6}$$

where p_{pe}^{defn} is the percentage of plastic events that localize on defects or nearest neighbors and p^{defn} is the percentage of global defects, i.e., the ratio between the number of defects or nearest neighbors of defects and the number of atoms. By using definition (6) we can follow the evolution of the correlation between plastic rearrangements and defects as a function of the applied strain. If $C(\epsilon_i) > 1$ the plastic events at strain ϵ_i are preferentially localized on defects or nearest neighbors of defects. A value of $C(\epsilon_i) < 1$ means that plastic events tend to avoid these sites. If $C(\epsilon_i) = 1$ the plastic events and the defects at strain ϵ_i have no explicit correlation. The evolution of $C(\epsilon_i)$ for different values of λ and for different quenching rates is shown in Figs. 11(a) and 11(b), respectively. The large fluctuations displayed by the curves in Fig. 11 at low strains are due to the fact that only few plastic events occur at small shear strains, while the statistics is better for larger strains. The initial correlation decreases by increasing the applied strain and at the yield point the curves tend to flatten. The plateau at large strains is generally an increasing function of λ (or a decreasing function of the quenching rate), indicating that correlations between plastic rearrangements and defects are stronger for a larger three-body term and/or for a more ordered structure. For lower values of λ and/or higher quenching rates, the larger number of defects present in the structure (see Fig. 9) makes the correlation unclear between the localization of plastic events and defects. In fact, for $\lambda = 17$ it can be seen that a value of $C \simeq 1$ is approached at high shear strains, i.e., the connection between plastic events and structural defects becomes blurred. This is even clearer for the highest quenching rate we have considered in Fig. 11(b), for which the correlation function is practically constant and very close to 1 for the whole strain range. For the other values of λ we have studied $C > 1$ over the whole range of strains, meaning that plastic events tend to localize preferentially close to defects. Instead, the effect of the quenching rate on the localization is weaker: for the quenching rates we have considered in Fig. 11(b) only the smallest reveals an appreciable correlation, while values of C close to 1 are approached at larger quenching rates.

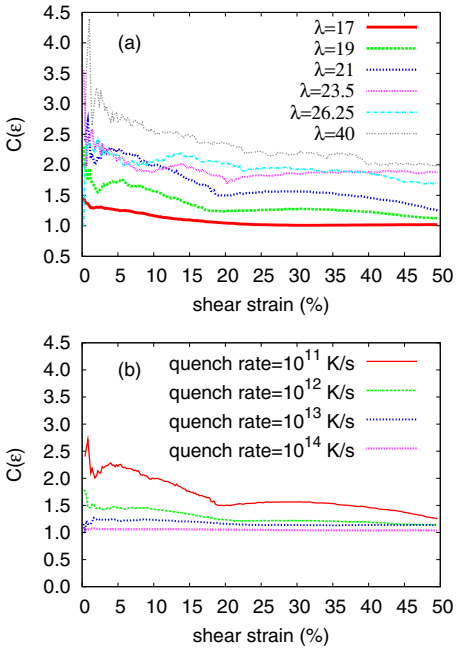

FIG. 11. (Color online) Correlation function between plastic events and defects, as defined in Eq. (6), as a function of the applied shear strain for different values of λ for a A-Si system prepared with a quenching rate of 10^{11} K/s (a) and for different quenching rates with $\lambda = 21$ (b).

VII. DISCUSSION AND CONCLUSIONS

The mechanical response of disordered systems at small scales has a broad range of applications, ranging from the elaboration of materials for nanoelectronic devices with controlled microstructure, to the prediction of damage in macromolecular glasses and granular assemblies. In this paper, we insist on the role played by local order on the plastic response of amorphous solids. We have seen that a systematic increase of the three-body interactions through the parameter λ in the empirical interatomic potential used to generate our systems induces a monotonous change in the mechanical response of the system: increase of the yield stress and of the yield strain, decrease of the average size of the plastic events, decrease of the cumulative number of plastic event, increase of the energy dissipated at the yield stress with a strong localization of the plastic rearrangements and heterogeneous flow, systematic increase of the spatial correlation between local plastic rearrangements, and structural defects. An analogous dependence can be seen by decreasing the quenching rate at a given value of λ, although it is less sensitive.

This behavior can be qualitatively compared with the Peierls-Nabarro description of plasticity in crystals, where the *width* of the dislocation, and thus the directionality of bonds, is shown to play a crucial role in the yield stress. We have shown here that the Peierls-Nabarro description, involving the elastic constants and the width of the plastic events at the yield point, is in good agreement with our data

and allows to define a Burgers vector that is independent of λ as well as of the quenching rate. The Burgers vector is smaller but comparable to the bond length. The systematic decrease of the size of the plastic events when the three body term increases gives rise to a large increase of the yield stress as a function of the directionality of the bonds and of local order. This formal analogy with the Peierls-Nabarro theory in crystals suggests the existence of an underlying lattice in the amorphous material, and should be a challenge for further study. However, it must be noted that the diffusive dynamics of plastic events in amorphous materials, and the dynamics of dislocations is quite different, as already mentioned in [4].

Finally, the evolution of the total stress as a function of the applied strain thus appears as a consequence of the spatial organization of plastic events of different sizes: the stress released is a measurement of the energy dissipated during the irreversible process. However, the origin of this spatial organization is still lacking. We have shown in this paper that, while the spatial localization of plastic rearrangements can be related to the presence of a local structural defect (such as a coordination defect) for strong directionality of local bonds, such a correspondence cannot be clearly identified when the directionality of the local bonds is low. In a previous paper [10], we have shown that for pure two-body interactions, as in Lennard-Jones glasses, there is no simple connection between the presence of this kind of structural defect and the occurrence of a plastic event at that place. Other people have proposed to look to other kinds of structural changes, like the "bound directionality," but it is not clear whether these structural changes are at the origin, or are the consequences of plastic rearrangements [13]. Moreover, the usual criterion of plasticity involving stress components (von Mises, Tresca, Druger-Prager) are not valid at small scale. The best local criterion of plasticity in Lennard-Jones glasses involved a measurement of the local Elastic Moduli [10]. It would be interesting to study now the validity of all these criteria as a function of the local order, as monitored by λ and by the quenching rate. This would also help us to understand the dynamics of the plastic events in the system.

This work has been done at very small temperature, in order to enhance the effect of the geometrical disorder on the mechanical response of amorphous solids. It is sufficient for example to describe the mechanical response of macroscopic assembly of beads, such as colloidal systems [33]. For molecular glasses, the effect of the temperature can be very important and will deserve further study.

ACKNOWLEDGMENT

A PEPS-PTI financial support from CNRS (France) is acknowledged.

[1] D. François, A. Pineau, and A. Zaoui, *Mechanical Behavior of Materials* (Kluwer Academic Publisher, Dordrecht, 1998).
[2] R. Peierls, Proc. Phys. Soc. London **52**, 34 (1940).
[3] F. R. N. Nabarro, Proc. Phys. Soc. London **59**, 256 (1947).
[4] A. Tanguy, F. Leonforte, and J.-L. Barrat, Eur. Phys. J. E **20**, 355 (2006).
[5] A. S. Argon, Acta Metall. **27**, 47 (1979).
[6] M. L. Falk and J. S. Langer, Phys. Rev. E **57**, 7192 (1998).
[7] P. Sollich, Phys. Rev. E **58**, 738 (1998).
[8] L. Bocquet, A. Colin, and A. Ajdari, Phys. Rev. Lett. **103**, 036001 (2009); J. Goyon, A. Colin, G. Ovarlez, A. Ajdari, and L. Bocquet, Nature (London) **454**, 84 (2008).
[9] M. Tsamados, A. Tanguy, F. Leonforte, and J.-L. Barrat, Eur. Phys. J. E **26**, 283 (2008).
[10] M. Tsamados, A. Tanguy, C. Goldenberg, and J.-L. Barrat, Phys. Rev. E **80**, 026112 (2009).
[11] A. Lemaître and C. Caroli, Phys. Rev. Lett. **103**, 065501 (2009).
[12] J. C. Baret, D. Vandembroucq, and S. Roux, Phys. Rev. Lett. **89**, 195506 (2002); M. Talamali, V. Petaja, S. Roux, and D. Vandembroucq, e-print arXiv:1005.2463.
[13] F. Albano and M. Falk, J. Chem. Phys. **122**, 154508 (2005); Y. Shi and M. L. Falk, Phys. Rev. B **73**, 214201 (2006); Y. Q. Cheng, A. J. Cao, H. W. Sheng, and E. Ma, Acta Mater. **56**, 5263 (2008).
[14] J. Rottler and M. O. Robbins, Phys. Rev. E **68**, 011507 (2003); Comput. Phys. Commun. **169**, 177 (2005).
[15] M. J. Demkowicz and A. S. Argon, Phys. Rev. Lett. **93**, 025505 (2004).
[16] F. Spaepen, Acta Metall. **25**, 407 (1977).
[17] A. V. Granato and V. A. Khonik, Phys. Rev. Lett. **93**, 155502 (2004).
[18] C. L. Rountree, D. Vandembroucq, M. Talamali, E. Bouchaud, and S. Roux, Phys. Rev. Lett. **102**, 195501 (2009).
[19] V. A. Khonik, Yu. P. Mitrofanov, S. A. Lyakhov, D. A. Khoviv, and R. A. Konchakov, J. Appl. Phys. **105**, 123521 (2009).
[20] Byung-Gil Yoo, Kyoung-Won Park, Jae-Chul Lee, U. Ramamurty, and Jae-il Jang, J. Mater. Res. **24**, 1405 (2009).
[21] R. Bhowmick, R. Raghavan, K. Chattopadhyay, and U. Ramamurty, Acta Mater. **54**, 4221 (2006).
[22] Y. T. Zhang, J. L. Qiao, and T. Ao, Modell. Simul. Mater. Sci. Eng. **15**, 147 (2007).
[23] F. Varnik, L. Bocquet, and J.-L. Barrat, J. Chem. Phys. **120**, 2788 (2004).
[24] F. H. Stillinger and T. A. Weber, Phys. Rev. B **31**, 5262 (1985).
[25] J. Tersoff, Phys. Rev. B **38**, 9902 (1988).
[26] M. Talati, T. Albaret, and A. Tanguy, EPL **86**, 66005 (2009).
[27] M. Ishimaru, S. Munetoh, and T. Motooka, Phys. Rev. B **56**, 15133 (1997).
[28] T. S. Majmudar and R. P. Behringer, Nature (London) **435**, 1079 (2005).
[29] J. Nocedal and S. J. Wright, *Numerical Optimization* (Springer, New York, 2006), see in particular procedure 3.1 on p. 41.
[30] H. J. C. Berendsen, J. P. M. Postma, W. F. van Gunsteren, A. Di Nola, and J. R. Haak, J. Chem. Phys. **81**, 3684 (1984).
[31] M. J. Demkowicz and A. S. Argon, Phys. Rev. B **72**, 245205 (2005).

[32] K. Laaziri, S. Kycia, S. Roorda, M. Chicoine, J. L. Robertson, J. Wang, and S. C. Moss, Phys. Rev. Lett. **82**, 3460 (1999).
[33] M. Tsamados, Eur. Phys. J. E **32**, 165 (2010).
[34] S. J. Plimpton, J. Comput. Phys. **117**, 1 (1995), see also http://lammps.sandia.gov.
[35] C. Goldenberg and I. Goldhirsch, Granular Matter **6**, 87 (2004).
[36] R. F. W. Bader, Chem. Rev. **91**, 893 (1991).
[37] T. Albaret, F. Finocchi, and C. Noguera, Faraday Discuss. **114**, 285 (1999); W. Tang, E. Sauville, and G. Henkelman, J. Phys.: Compute Mater. **21**, 084204 (2009).
[38] Note that for $\lambda=0$, corresponding to pure two-body interactions, this is not the case as seen in Lennard-Jones glasses where the average environment of the atoms remains the same during the shear deformation [4,10].
[39] The parameters used for the intensity differences and for the nonaffine displacements have been chosen by comparing the variations of the total PE(r) energy integrated over all the basins and the total dissipated energy as a function of strain. It shows a very good qualitative agreement between them, even after a change by a factor 2 of any of these parameters. Note that the total number of plastic events would be slightly affected by the suppression of one of the parameters used to identify the pertinent basins, but neither the cumulative plastic energy (Fig. 7), nor the conclusions about the correlation function between plastic events and defects (Fig. 11) are changed.